

Modeling Spiral Inductors in SOS Processes

William B. Kuhn, *Senior Member, IEEE*, Xin He, *Student Member, IEEE*, and Mohammad Mojarradi, *Member, IEEE*

Abstract—Existing models for simulating spiral inductors fabricated in Silicon processes are outgrowths of the PI structure originally employed by Nguyen and Meyer. This structure and its subsequent elaborations work well for inductors in which the dominant loss mechanism is the underlying substrate. For newer processes with very high resistivity or insulating substrates such as Silicon-on-sapphire however, the model breaks down since inductor quality factor Q is then determined predominantly by series trace resistance. Models suitable for use in such processes are proposed and compared with measured data. The new models contain only four to six elements and, unlike the classic PI model, provide a broadband match to measured impedance behavior in both differentially driven and single-ended circuit applications.

Index Terms—Eddy currents, inductors, modeling, silicon-on-insulator (SOI) technology, SPICE.

I. INTRODUCTION

IN 1990, Nguyen and Meyer [1] were among the first to suggest practical applications for spiral inductors in Silicon processes and to provide an equivalent circuit for SPICE-type simulation. Their original six-element PI model in Fig. 1(a) reasonably approximated all major performance parameters, including low frequency inductance and trace resistance, self-resonant frequency (SRF), and quality factor (Q) versus frequency. Since this circuit was introduced, the PI structure has remained the basis for virtually all subsequent models, although additional elements have been added as inductors have been examined and understood in greater detail [2]–[4]. The now pervasive nine-element circuit of Fig. 1(b) adds a capacitance to account for complex permittivity in the substrate and a shunt capacitance to improve SRF modeling. Subsequent models have added elements to emulate eddy-current losses within the substrate [5]–[8] and skin effect and/or current crowding [9]–[14], and may contain up to 22 elements [15].

In this paper, we propose simplified models for advanced integrated circuit (IC) processes aimed at radio frequency IC (RFIC) design. These processes offer very high resistivity substrates in an effort to reduce or eliminate substrate losses. When substrate losses are reduced to negligible values, it becomes appropriate to consider a departure from the classic PI structure. We show how inductor performance can then be competently represented with either a simple three-element

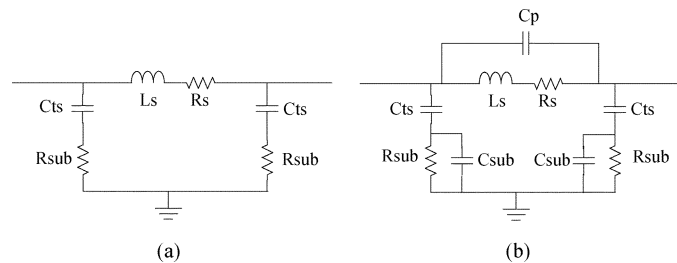


Fig. 1. Classic PI-type spiral inductor models.

frequency-dependent model, or with four, five, or six-element SPICE-compatible models. Development of the frequency dependent model provides a direct representation of Q -limiting effects while the SPICE-compatible models allow simulation with a large base of design tools. In contrast to using raw S -parameters directly in simulation (when permitted by a tool), the models offer a circuit-level view that is useful to an engineer during the design phase. The models have been validated against measured results from a large array of inductors in Silicon-on-sapphire (SOS) where Q is limited only by dc series resistance and skin-effect/current-crowding mechanisms. Representative results are presented, together with a comparison between the new models and the classic PI structure.

II. SPIRAL INDUCTOR LOSS MECHANISMS AND Q

Arguably, one of the most important performance parameters of a spiral inductor is its quality factor Q . This parameter can affect a host circuit's bandwidth, phase noise, noise figure, power efficiency, etc., and should be accurately represented at all frequencies for a model to be of general use.

By defining Q in terms of power dissipation

$$Q = \frac{2\pi(\text{Peak Energy Stored})}{\text{Energy Lost Per Cycle}} \quad (1)$$

it can be shown that when multiple independent losses are present, the net inductor Q can be expressed as

$$Q_L = \frac{1}{\frac{1}{Q_1} + \frac{1}{Q_2} + \dots} \quad (2)$$

where Q_i represents the quality factor that would be obtained if only the i^{th} loss mechanism was present. From (2), it is clear that when one Q_i is significantly lower than the others, it will dominate as well as upperbound the overall inductor Q .

As illustrated in Fig. 2, an inductor fabricated in a typical CMOS process is limited by several loss mechanisms and their respective Q_s , including:

- 1) I^2R losses from displacement currents conducted through the trace-to-substrate capacitances C_{ts} and underlying resistive substrate (leading to $Q_{\text{sub-disp}}$),

Manuscript received October 22, 2003; revised February 6, 2004. This work was supported in part by the National Science Foundation under Grant ECS-9875770, and by the Jet Propulsion Laboratory, California Institute of Technology, under a contract with the National Aeronautics and Space Administration. The review of this paper was arranged by Editor J. N. Burghartz.

W. B. Kuhn and X. He are with Kansas State University, Department of Electrical and Computer Engineering, Manhattan, KS 66506-5204 USA.

M. Mojarradi is with the Jet Propulsion Laboratory, California Institute of Technology, Pasadena, CA 91125 USA.

Digital Object Identifier 10.1109/TED.2004.826868

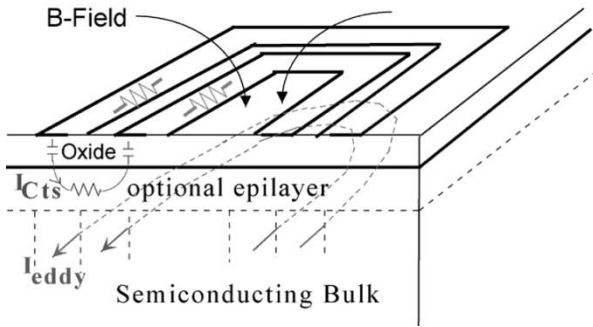


Fig. 2. Cross-sectional view of inductor in typical Si process.

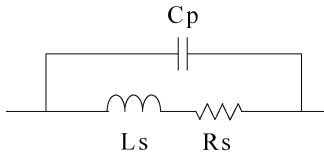


Fig. 3. Simplified three-element model.

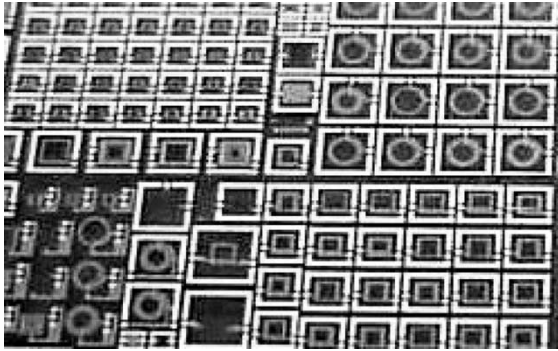


Fig. 4. Spiral inductor array in SOS used for model development/validation.

- 2) I^2R losses in the substrate from eddy currents I_{eddy} circulating below the spiral turns due to the inductor's magnetic field (leading to $Q_{\text{sub-eddy}}$), and
- 3) I^2R losses in the metal traces (leading to Q_{metal}).

To date, most inductors have been primarily limited by $Q_{\text{sub-disp}}$ and/or $Q_{\text{sub-eddy}}$, with resulting max- Q_L values of around 3 in epi-processes with $<0.02 \Omega\cdot\text{cm}$ substrate bulk-resistivity and around 8 to 12 in processes with 10 to 20 $\Omega\cdot\text{cm}$ non-epi-substrates [6]. With the introduction of silicon-on-insulator (SOI) processes with very high resistivity substrates and SOS with an insulating substrate, losses leading to Q_{sub} can be largely or totally eliminated, together with the circuit elements of the PI model used to simulate them. A model that represents metal losses alone is then desired. A good starting point for such a model is the PI circuit of Fig. 1(b) with the six substrate-related elements removed.

III. FREQUENCY DEPENDENT THREE-ELEMENT MODEL

A simple three-element model for inductors in which Q_{metal} dominates is shown in Fig. 3. Here, L_s and C_p model the low frequency inductance and self-resonance effects, while R_s models resistive losses in the metal traces that form the spiral itself.

While L_s and C_p are determined mainly by the spiral's geometry and should be relatively constant parameters, the effective resistance of the spiral's traces R_s is known to increase dramatically with frequency [9]–[11]. This increase derives from current crowding, which, roughly speaking, restricts the effective width of the trace, and from skin effect which restricts its thickness. At frequencies below 2 GHz, current crowding typically dominates and exhibits a behavior given by [10]

$$R_s \approx R_{\text{DC}} \left[1 + 0.1 \left(\frac{\omega}{\omega_{\text{crit}}} \right)^2 \right] \quad (3)$$

where R_{DC} is the low-frequency resistance value and ω_{crit} determines the frequency at which the increase begins. At ω_{crit} , the resistance rises to 110 percent of its dc value. Above ω_{crit} , resistance builds quadratically initially, and then slows its rate of increase to approximately linear at a frequency ω_{lim} [10]. In contrast, classic skin-effect theory alone predicts an increase proportional to $\sqrt{\omega}$ beginning above about 2 GHz (depending on trace thickness).

To test the validity of the constant L_s , C_p assumption and to verify the predicted behavior of R_s , the model of Fig. 3 was fit to measured data from a large array of inductors fabricated in a SOS process (Fig. 4). The fitting was performed using the following procedure.

- 1) Convert measured S-parameter data into impedance values $Z(\omega)$.
- 2) Plot *apparent* inductance L_{app} found from $\text{Im}(Z)/\omega$.
- 3) Find L_s from the low frequency value of L_{app} .
- 4) Find SRF from the frequency where L_{app} becomes negative.
- 5) Compute C_p from L_s and SRF.
- 6) Find the impedance $Z_{\text{RL}}(\omega)$ of the series-connected components R_s , L_s by converting $Z(\omega)$ to $Y(\omega)$, subtracting off the admittance of C_p , and converting back to impedance.
- 7) Plot the real and imaginary parts of $Z_{\text{RL}}(\omega)$ as R_s and L_s .

A representative result is shown in Fig. 5 for a 14-nH, 250- μm , eight-turn spiral. R and L values both before and after subtracting out C_p effects are displayed to emphasize the difference between their apparent and actual values found from $Z(\omega)$ and $Z_{\text{RL}}(\omega)$ respectively. Note that the final L_s curve with C_p removed is flat, indicating that both C_p and L_s in Fig. 3 can indeed be constant in the model. R_s shows the expected quadratic increase predicted by the theory of current crowding, which unfortunately lowers the Q and makes the model unsuitable for use with circuit simulators, which lack a frequency dependent resistance element.

IV. ACTUAL VERSUS APPARENT Q

While the frequency dependent nature of the three-element model makes it problematic for simulation, it is very useful for finding inductor Q . In the literature, an inductor's Q is most often plotted as the simple ratio

$$Q = \frac{\text{Im}(Z)}{\text{Re}(Z)}. \quad (4)$$

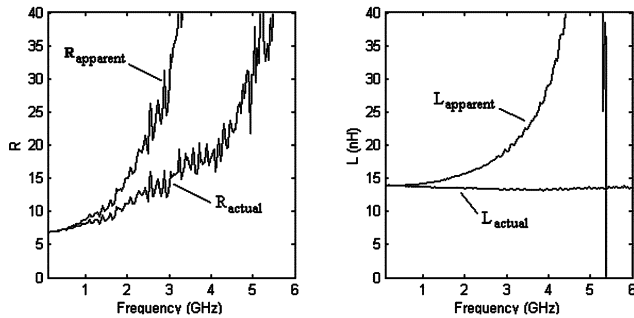


Fig. 5. Resistance and inductance from measurements of 14-nH spiral before and after removing effects of C_p .

Unfortunately, this leads to $Q = 0$ at self-resonance, which is inconsistent with (1) since the inductor is still storing and exchanging energy with its built-in capacitance. When taken at face value, this *apparent- Q* from (4) leads to incorrect host-circuit performance predictions in some applications. For example, when used in a bandpass filter operating near the inductor's SRF, a low (or zero) Q would predict a wide (infinite) bandwidth, whereas the actual bandwidth obtained may be much less. Using the model of Fig. 3 however, the actual- Q (energy storage-based) can be easily found from the frequency dependent R_s values as

$$Q_{true} = \frac{\text{Im}(Z_{RL})}{\text{Re}(Z_{RL})} = \frac{\omega L_s}{R_s}. \quad (5)$$

An example result derived from the data in Fig. 5 is shown in Fig. 6. Note that the actual- Q near resonance exceeds 12, in contrast to values close to zero predicted by (4).

V. FREQUENCY INDEPENDENT FIVE-ELEMENT MODEL

To develop a model suitable for use in SPICE-like circuit simulators, the frequency dependent resistance element in Fig. 3 must be eliminated. Following [10], this can be done by borrowing from a technique used to simulate eddy-current losses in the substrate [5]–[8] consisting of a coupled LR loop as illustrated in Fig. 7.

Here, L_c and R_c model current-crowding losses within the metal traces, and hence, the observed increase in effective series resistance with frequency. The impedance of the R_s , L_s series-connected components in Fig. 7 is modified to [7]

$$Z_{R_s L_s} = R_{dc} + j\omega L_s + \frac{\omega^2 M^2}{R_c + j\omega L_c} \quad (6)$$

which shows a quadratically increasing real part up to a relaxation frequency R_c/L_c , matching the basic first-order behavior of current crowding described in [10]. To fit this model to the quadratic increase in R suggested by (3), we need to determine L_c , R_c , and the mutual inductance M (or coupling-coefficient k). From measured data such as that in Fig. 5, we can estimate the critical frequency ω_{crit} where the resistance rises to 110 percent of its dc value and the frequency ω_{lim} where the quadratic increase slows. Then, from (6), we solve

$$\frac{(\omega_{crit} M)^2}{R_c} = 0.1 R_{dc} \quad (7)$$

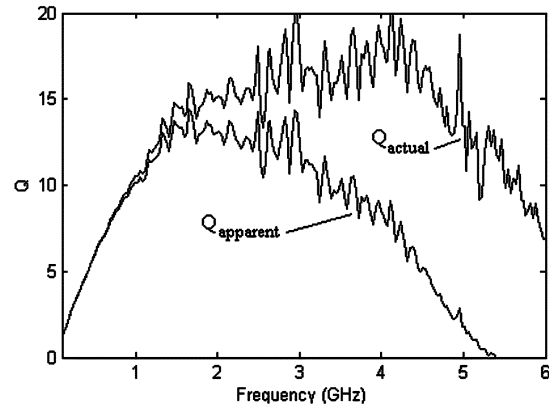


Fig. 6. Actual- versus apparent- Q of 14-nH, 250-um inductor.

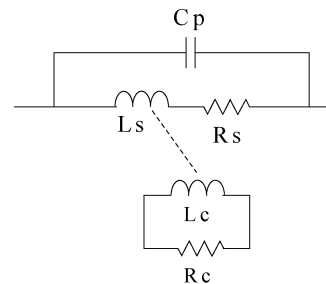


Fig. 7. Frequency independent five-element model.

and

$$\omega_{lim} = \frac{R_c}{L_c} \quad (8)$$

for the desired component values. Here, R_{dc} is defined as the real part of $Z_{RL}(\omega)$ at $\omega = 0$. Since there are 3 unknowns and only two constraints, we must fix one value arbitrarily. For example, selecting $L_c = \alpha L_s$ with α as a constant, we find

$$R_c = \alpha \omega_{lim} L_s \quad (9)$$

and

$$M = \sqrt{\frac{0.1 R_s R_c}{(\omega_{crit})^2}} \quad (10)$$

$$k = \frac{M}{\sqrt{L_s L_c}}. \quad (11)$$

For the previously discussed inductor with ω_{crit} and ω_{lim} estimated as $2\pi(900 \text{ MHz})$ and $2\pi(10 \text{ GHz})$, and with $\alpha = 0.1$ (to provide some physical significance since the total area in the eddy-loops is smaller than the total inductor area), we find $L_c = 1.4 \text{ nH}$, $R_c = 88 \Omega$, and $k = 0.32$. A comparison between the resulting lumped element model and measured results is shown in Fig. 8. Plots of Q and R computed from (4) and (5) both show good agreement with measured results from dc up through the inductor's SRF of 5.5 GHz. Note that the actual- Q

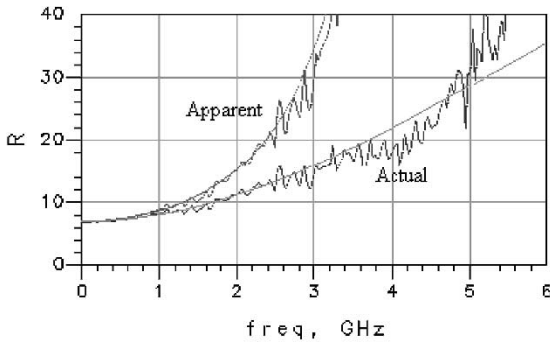


Fig. 8. Comparison of measured results versus five-element model impedance.

curves are more sensitive to measurement system and/or modeling errors than the typically used apparent- Q curves, providing a better check on behavior near SRF.¹

VI. SIMPLIFIED FREQUENCY-INDEPENDENT FOUR-ELEMENT MODEL

The five-element model of Fig. 7 provides good agreement with measured results, but can be simplified in the case where measured R increases only quadratically over the frequency range of interest. The nearly equivalent model shown in Fig. 9 is easier to work with in hand analysis of RF circuits, and is also helpful in comparing results to the classic PI structure.

For this model, the impedance of the R_s , L_s components in parallel with R_p (excluding C_p) is

$$\begin{aligned} Z_{R_s L_s R_p} &= \frac{(R_s + j\omega L_s)R_p}{(R_s + j\omega L_s) + R_p} \\ &= \frac{R_s R_p (R_s + R_p) + (\omega L_s)^2 R_p}{(R_s + R_p)^2 + (\omega L_s)^2} \\ &\quad + j\omega L_s \frac{R_p^2}{(R_s + R_p)^2 + (\omega L_s)^2} \end{aligned} \quad (12)$$

which can be simplified by noting that for high Q inductors (e.g., $Q > 10$), $R_p \gg R_s$ and $R_p \gg \omega L_s$ so that

$$Z_{R_s L_s R_p} \approx R_s + \omega^2 \frac{L_s^2}{R_p} + j\omega L_s. \quad (13)$$

Equation (13) shows the desired quadratic increase in R with frequency and can be fit to measured data by setting the middle term equal to $0.1 R_s$ at the critical frequency, yielding

$$R_p = 10 \omega_{\text{crit}}^2 \frac{L_s^2}{R_s}. \quad (14)$$

For the sample inductor, the resulting value is $R_p = 8 \text{ k}$ and the model fit is illustrated in Fig. 10. Note that the curves are nearly identical to those in Fig. 8 with the exception of slightly lower values of Q at higher frequencies.

¹The peaking near 4 GHz in the actual- Q curve is more noticeable than in the apparent- Q curve. This peaking is believed to be from measurement system limitations. At large Q , very small errors in measured reflection coefficient can lead to such variations even after careful network analyzer calibration.

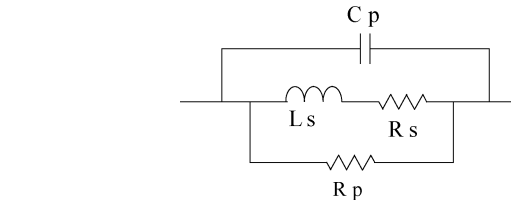
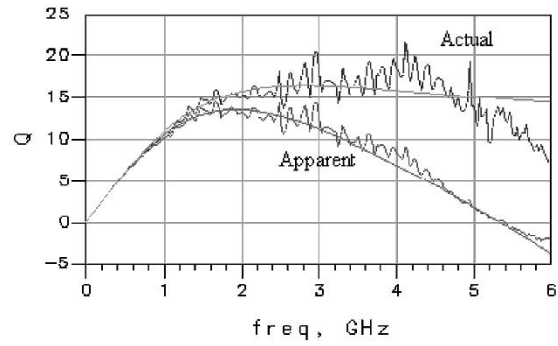


Fig. 9. Simplified four-element model.

VII. COMPARISON WITH CLASSIC PI MODEL

Comparing the simplified four-element model of Fig. 9 with the classic PI models of Fig. 1, we note both similarities and differences. First, both effectively model the decrease in Q at high frequencies (relative to an ideal inductor with the same dc resistance) using shunt resistance. Similarly, both represent self-resonance behavior using shunt capacitance. However, the PI model contains a ground connection that has no physical basis when applied to SOI processes with very high resistivity substrates. This ground connection can, in some cases, significantly degrade the model's accuracy.

As an example, Fig. 11 shows a PI model fit to the sample inductor, together with the simplified four-element model discussed above. Comparing the circuits we note that the series combination of the two substrate resistors in the PI model is equal to the single R_p element of the four-element model, as would be expected from theory. The value of C_{ts} in the PI circuit is found to be noncritical, with 100 fF to several picofarads giving similar results.

To examine the suitability of each model for simulating RFIC circuits, the impedance of LC tanks in the oscillator designs of Fig. 12 are considered. In Fig. 12(a) a single tank inductor is operated in a differential mode while in Fig. 12(b), two inductors are employed with one end of each inductor ac grounded. Fig. 13 plots the tank-circuit impedance (14-nH inductor in parallel with 220 fF) predicted by the models of Fig. 11 for each configuration, together with the impedance found directly from a measured S -parameter two-port element with 220 fF shunt. In both cases, the new model provides a reasonably accurate fit to the two-port S -parameter-based simulation result, while for the PI model, the tank circuit resistance and bandwidth are incorrect for the application where one side of the inductor is ac grounded. This is basically due to shorting out of C_{ts} and R_{sub} on one side of the model, leading to a decrease in shunt resistance and hence, Q . This in turn leads to incorrect assessment

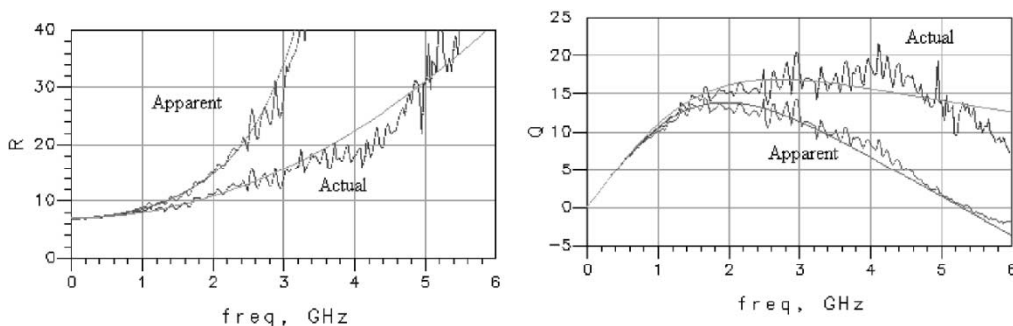


Fig. 10. Comparison of measured results with four-element model.

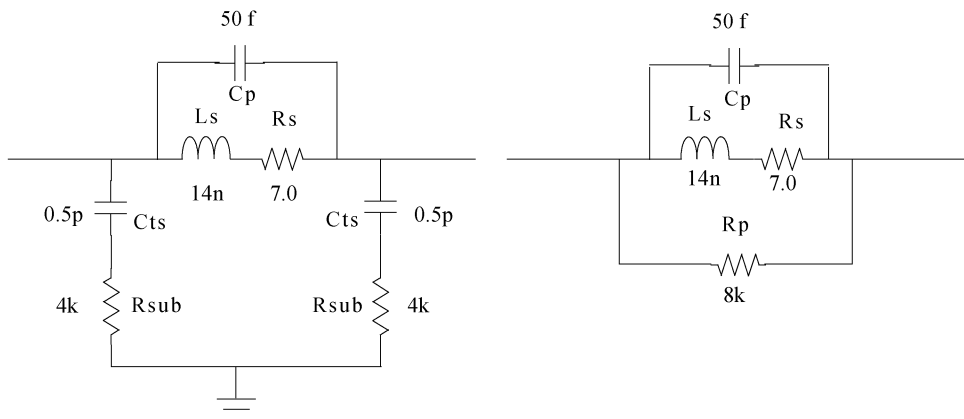


Fig. 11. PI model and simplified four-element model of 14 nH example inductor.

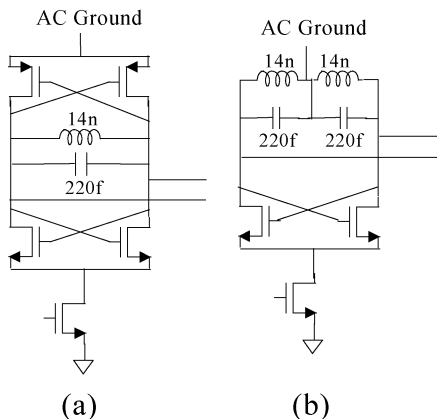


Fig. 12. Typical application circuits. (a) Differentially driven LC tank. (b) Single-ended LC tank.

of oscillator phase-noise performance and of the negative resistance required in the design.

While the problem illustrated here could be “fixed” by modifying R_{sub} in Fig. 11(a) to 8 k, the resulting PI model would then only be appropriate for use in the single-ended mode—a difficulty that the new models do not share. As previously noted, this is a consequence of the ground node within the PI structure which has no physical basis when substrate losses are eliminated.

VIII. AN IMPROVED HIGHER-ORDER MODEL

Although the results in Figs. 8, 10, and 13 show a good model fit for the 250- μ m example inductor, matching the behavior of

physically larger, higher performance spirals in the test array of Fig. 4 was found to be difficult. For example, when applied to a 600- μ m high- Q ($Q > 30$) spiral, the five-element model would match well over dc to 3 GHz, or 3 to 6 GHz, but not over the full dc to 6-GHz frequency range. The solution to this problem is to introduce additional degrees of freedom by adding circuit elements to the model. This is essentially what the nine-element model of Fig. 1(b) offers relative to the original seven-element Nguyen and Meyer design in Fig. 1(a).

An obvious extension of the models presented so far in this paper is to combine the topologies of Figs. 7 and 9 to form the six-element model shown in Fig. 14.² This combination is motivated by the observation that L_c and R_c can handle the low-frequency current-crowding behavior while the addition of R_p can then emulate the combined crowding and skin-effect behavior at higher frequencies.

Representative results for a 2.2-nH, 600- μ m, 1.25-turn spiral in SOS are shown in Fig. 15, together with curves from the measured data and a curve from the simpler four-element model. The results from the six-element model were achieved using $\omega_{crit} = 2\pi(350 \text{ MHz})$ and $\omega_{lim} = 2\pi(1 \text{ GHz})$ in (9) through (11) to create the initial observed rise in resistance and an R_p value chosen for best fit to R and Q behavior above 3 GHz. Final values were $L_s = 2.2 \text{ nH}$, $R_s = 0.5\Omega$, $C_p = 29 \text{ fF}$, $L_c = 210\text{pH}$, $R_c = 1.35\Omega$, $k = 0.17$, and $R_p = 5 \text{ k}\Omega$.

²Another possibility would be to create multiple eddy loops as suggested by equations in [7].

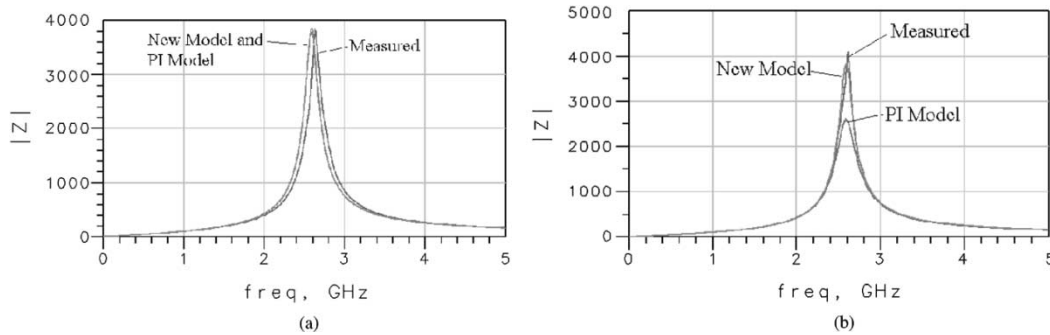


Fig. 13. Simulated impedances from models versus measured S-parameter result. (a) Differentially driven. (b) Single-ended.

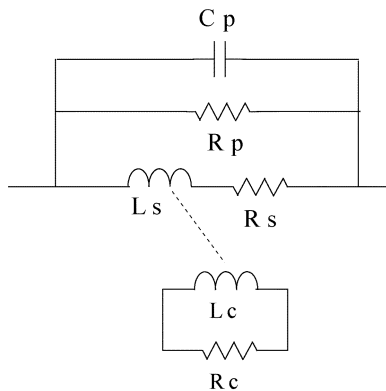


Fig. 14. Improved six-element model.

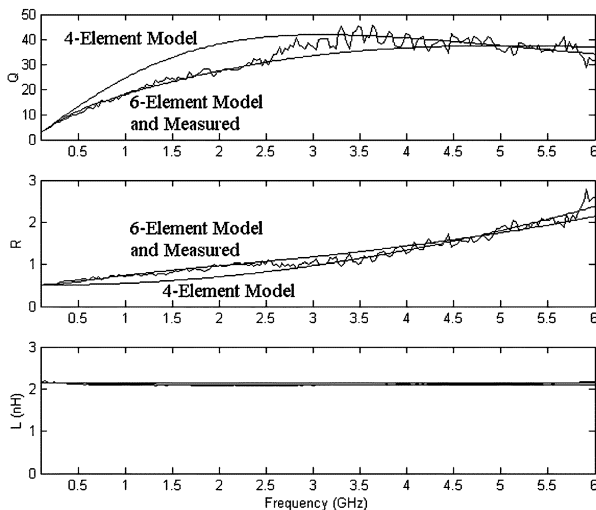


Fig. 15. Comparison of measured values to simulation using five- and six-element models for larger 600-um high-performance spiral in SOS.

IX. SUMMARY AND CONCLUSION

To date, RF circuit designers have used various elaborations of the PI model of Nguyen and Meyer to simulate circuits employing spiral inductors. These models serve well for inductors in which the primary loss mechanism is the substrate, but are less accurate for inductors created in newer RF-compatible processes with very high-resistivity bulk material such as SOS. The simple four- and five-element frequency independent models of Fig. 7 and 9 provide a good fit to measured data taken from small-to-moderate sized (<300 um) inductors fabricated in SOS. They both accurately model the quadratic increase in

resistance versus frequency from current crowding while the five-element version offers the ability to fit to cases where this increase slows to linear above a limiting frequency. For larger, high- Q spirals (e.g. 600 um, $Q > 30$), the six-element model of Fig. 14 has been found to perform well, modeling current crowding below 2 GHz and combined crowding plus skin effect through 6 GHz. These models work well in both differential and single-ended applications, unlike the classic PI circuit, since they do not artificially introduce a ground node. While validation of the new models in other SOI processes with very high resistivity but noninsulating substrates is still needed, the models can be expected to perform well, to the extent that substrate loss is reduced to negligible values relative to trace resistance loss.

ACKNOWLEDGMENT

The authors would like to thank D. Nobbe, D. Kelly, and J. Holden at Peregrine Semiconductor for access to the experimental inductor array, and for helpful comparisons with models published to date.

REFERENCES

- [1] N. M. Nguyen and R. G. Meyer, "Si IC-compatible inductors and LC passive filters," *IEEE J. Solid-State Circuits*, vol. 25, pp. 1028–1031, Aug. 1990.
- [2] J. N. Burghartz, M. Soyuer, and K. A. Jenkins, "Microwave inductors and capacitors in standard multilevel interconnect silicon technology," *IEEE Trans. Microwave Theory Tech.*, vol. 44, pp. 100–104, Jan. 1996.
- [3] J. R. Long and M. A. Copeland, "The modeling, characterization, and design of monolithic inductors for silicon RF ICs," *IEEE J. Solid-State Circuits*, vol. 32, pp. 357–369, Mar. 1997.
- [4] C. P. Yue and S. S. Wong, "Physical modeling of spiral inductors on silicon," *IEEE Trans. Electron Devices*, vol. 47, pp. 560–568, Mar. 2000.
- [5] P. Arcioni, R. Castello, L. Perregrini, E. Sacchi, and F. Svelto, "An improved lumped-element equivalent circuit for on silicon integrated inductors," in *Proc. RAWCON*, Aug. 9–12, 1998, pp. 301–304.
- [6] W. B. Kuhn and N. K. Yanduru, "Spiral inductor substrate loss modeling in silicon RF ICs," in *Proc. RAWCON*, Aug. 9–12, 1998, pp. 305–308.
- [7] D. Melendy, P. Francis, C. Pichler, K. Hwang, G. Srinivasan, and A. Weisshaar, "A new wideband compact model for spiral inductors in RFICs," *IEEE Electron Device Lett.*, vol. 23, pp. 273–275, May 2002.
- [8] J. N. Burghartz and B. Rejzai, "On the design of RF spiral inductors on silicon," *IEEE Trans. Electron Devices*, vol. 50, pp. 718–729, Mar. 2003.
- [9] J. Craninckx and M. S. J. Steyaert, "A 1.8-GHz low-phase-noise CMOS VCO using optimized hollow spiral inductors," *IEEE J. Solid-State Circuits*, vol. 32, pp. 736–744, May 1997.
- [10] W. B. Kuhn and N. M. Ibrahim, "Analysis of current crowding effects in multiturn spiral inductors," *IEEE Trans. Microwave Theory Tech.*, vol. 49, pp. 31–38, Jan. 2001.
- [11] J. Siero, J. M. Lopez-Villegas, J. Cabanillas, J. A. Osorio, and J. Samitier, "A physical frequency-dependent compact model for RF integrated inductors," *IEEE Trans. Microwave Theory Tech.*, vol. 50, pp. 384–392, Jan. 2002.

- [12] B.-L. Ooi, D.-X. Xu, P.-S. Kooi, and F. Lin, "An improved prediction of series resistance in spiral inductor modeling with eddy-current effect," *IEEE Trans. Microwave Theory Tech.*, vol. 50, pp. 2202–2206, Sept. 2002.
- [13] W. Y. Yin, S. J. Pan, Y. B. Gan, L. W. Li, and B. L. Ooi, "Global performance evaluation of various on-chip square spiral inductors on GaAs substrates," *Proc. Circuits, Devices, and Systems*, vol. 150, no. 1, pp. 51–56, Feb. 2003.
- [14] J. Gil and H. Shin, "A simple wide-band on-chip inductor model for silicon-based RF ICs," *IEEE Trans. Microwave Theory Tech.*, vol. 51, pp. 2023–2028, Sept. 2003.
- [15] Y. Cao, R. A. Groves, X. Huang, N. D. Zamdmer, J.-O. Plouchart, R. A. Wachnik, T.-J. King, and C. Hu, "Frequency-independent equivalent-circuit model for on-chip spiral inductors," *IEEE J. Solid-State Circuits*, vol. 38, pp. 419–426, Mar. 2003.



William B. Kuhn (S'78–M'79–SM'98) received the B.S. degree in electrical engineering from Virginia Polytechnic Institute and State University, Blacksburg, in 1979, the M.S. degree in electrical engineering from the Georgia Institute of Technology, Atlanta, in 1982, and the Ph.D. degree from Virginia Tech., in 1996.

From 1979 to 1981, he was with Ford Aerospace and Communications Corporation, Palo Alto, CA, where he designed radio receiver equipment, including frequency synthesizers and bit synchronizers. From 1983 to 1992, he was with the Georgia Tech Research Institute, Atlanta, working primarily in radar signal analysis and mixed-signal circuit simulator development. In 1996, he joined Kansas State University (KSU), Manhattan, as an Assistant Professor, later becoming an Associate Professor in 2000. He teaches courses in communications theory, radio and microwave circuit/system design, and VLSI. His research is primarily targeted at low-power radio electronics in CMOS, SOI, and GaAs technologies.

Dr. Kuhn is a recipient of a Bradley Fellowship in 1993 from Virginia Tech and a Faculty Early Career Development (CAREER) award from the National Science Foundation in 1999. He is also the recipient of the KSU Hollis Award for Excellence in Undergraduate Teaching in 2001, and the Eta Kappa Nu distinguished faculty award in 2002 and 2003.



Xin He (S'04) received the B.S. and M.E. degrees in instrumentation in 1997 and 2000 respectively, from the University of Science and Technology of China, Hefei, China. He received the M.S. degree in electrical engineering from the Kansas State University, Manhattan, in 2002, where he is currently pursuing the Ph.D. degree.

His research interests include RF filter design, high-efficiency power amplifiers, PLLs, and modeling of spiral inductors and varactors in SOI processes.



Mohammad Mojarradi (M'92) received the Ph.D. degree in electrical engineering from the University of California, Los Angeles (UCLA) in 1986.

Prior to joining Jet Propulsion Laboratory, Pasadena, CA, he was an Associate Professor at Washington State University, Pullman, and the Manager of the mixed-voltage/specialty integrated circuit group at the Xerox Microelectronics Center, El Segundo, CA. He is a Specialist in integrated mixed-signal/mixed-voltage electronic sensors, micromachined interface circuits, and mixed-mode integrated circuit design. He has more than 20 years of combined industrial and academic experience in his field. His current work focuses on developing highly efficient integrated mixed-signal electronics for sensors, actuators, and power management and distribution systems (PMAD) for avionics system on a chip for deep space using the SOI CMOS process.